Two-wavelength-difference measurement of gravitationally induced quantum interference phases

K. C. Littrell, B. E. Allman,* and S. A. Werner
Physics Department and Research Reactor Center, University of Missouri-Columbia, Columbia, Missouri 65211
(Received 4 April 1997)

One of the significant successes in the field of neutron interferometry has been the experimental observation of the phase shift of a neutron de Broglie wave due to the action of the Earth's gravitational field. Past experiments have clearly demonstrated the effect and verified the quantum-mechanical equivalence of gravitational and inertial masses to a precision of about 1%. In this experiment the gravitationally induced phase shift of the neutron is measured with a statistical uncertainty of order 1 part in 1000 in two different interferometers. Nearly harmonic pairs of neutron wavelengths are used to measure and compensate for effects due to the distortion of the interferometer as it is tilted about the incident beam direction. A discrepancy between the theoretically predicted and experimentally measured values of the phase shift due to gravity is observed at the 1% level. Extensions to the theoretical description of the shape of a neutron interferogram as a function of tilt in a gravitational field are discussed and compared with experiment. [S1050-2947(97)04109-7]

PACS number(s): 03.30.+p, 03.65.Bz, 04.80.−y, 07.60.Ly

I. INTRODUCTION

One of the fundamental ideas in modern physics is the equivalence principle, the idea that the effects of gravity and acceleration on the trajectory of a classical particle are locally indistinguishable. An analogous concept for quantum mechanics is the hypothesis that the wave function of a quantum-mechanical system in a uniform gravitational field **g** is indistinguishable from that of the same system moving with uniform acceleration $-\mathbf{g}$. Since the wave function is complex, it can be written as the product of a real probability amplitude and the exponential of an imaginary phase. The square of the probability amplitude of a quantum-mechanical particle is related to its density along the classical trajectory. The phase is related to the propagation of the particle's de Broglie wave and has no classical analog. Since detectors measure only particle densities, the phase of a matter wave is not directly observable. However, by using interferometric techniques similar to and based upon those for electromagnetic radiation, phase differences between matter wave subbeams can be measured.

The influence of gravity on the quantum-mechanical phase of the neutron de Broglie wave in a neutron interferometer was first observed by Colella, Overhauser, and Werner [1] in 1975 and then more accurately by Staudenmann *et al.* [2] in 1980, beginning a series of experiments of increasing sophistication of which this is the latest. These experiments, collectively known as COW experiments, are unique in that they involve the interaction of gravity with an intrinsically quantum-mechanical quantity and thus necessarily depend on both Planck's constant $\hbar$ and Newton's universal gravitational constant G [3]. This dependence allows the principle of equivalence to be studied in the quantum limit. Previous neutron experiments in which gravity was a consideration involve the deflection of particles by gravity and are thus essentially classical in nature.

The validity of the classical principle of equivalence has been verified to a very high precision [4]. Similarly, it has been demonstrated [5] that the probability density of the neutron in the Earth's gravitational field follows the same parabolic trajectory as a classical point particle with the same inertial mass to within an uncertainty of 3 parts in 10 000. The previous COW experiments have clearly demonstrated that a gravitational phase shift of the right magnitude exists, but later, more precise measurements [6,7] have shown disturbing discrepancies on the order of 1% between theory (including all known corrections) and experiment. Statistical errors and estimated and measured uncertainties in the experimental parameters are of order 1 part in 1000. The present work is an attempt to understand the reasons for these discrepancies.

Recently, Kasevich and Chu [8] have used an atomic fountain interferometer to measure the gravitational acceleration of atoms. They reported no significant discrepancies in an experiment with a resolution of 30 parts per 1×10^9, although a direct comparison with a locally measured value of the acceleration due to gravity **g** is not yet available.

In previous experiments, the effects of bending of the perfect Si crystal interferometer as it is tilted about the incident beam were measured by using x rays diffracting along approximately the same paths through the interferometer as the neutron beams. Since x rays are photons and thus massless and the gravitational redshift is negligibly small over the distances involved in these experiments, any phase shifts observed should be the result of bending of the interferometer as it is tilted about the incident beam. These x-ray phase shifts were then scaled to the neutron wavelength and used to compensate for bending effects in the neutron data. However, x rays are rather strongly absorbed in silicon and therefore sample a different region of the interferometer crystal blades than neutrons. The Borrmann fans within each crystal are fully illuminated in the neutron case, leading to a substantial spreading of the beam as it traverses the interferometer as schematically shown in Fig. 1. The tilt-induced phase of the x-ray interferogram has been shown to be a sensitive, nonlinear function of the position of the incident x-ray beam

*Present address: School of Physics, University of Melbourne, Parkville, Victoria 3052, Australia.

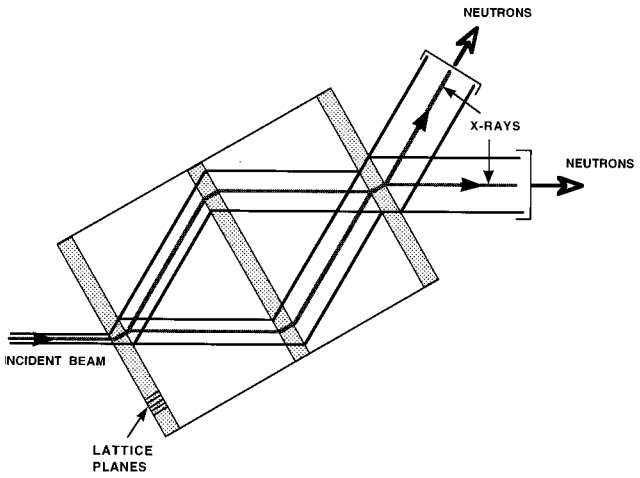

FIG. 1. Schematic diagram of a symmetric LLL perfect-crystal interferometer showing the spreading of the neutron beam by the Borrmann fans in each crystal plate. Since x rays experience substantial absorption in silicon, the rays traverse the interferometer via the anomalous transmission effect and do not spread out very much.

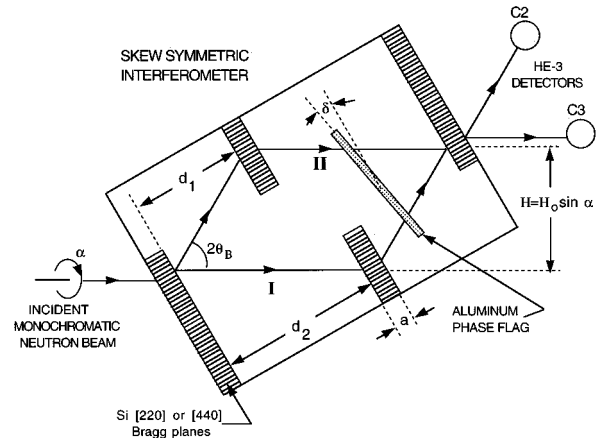

FIG. 2. A schematic diagram of the experimental arrangement. One sub-beam of the interferometer is raised above the other by tilting the interferometer an angle α about the incident beam. An additional phase shift due to the interaction of neutrons with matter can be introduced by rotating an aluminum phase shifter extending across both sub-beams through an angle δ.

on the first blade of the interferometer within the region illuminated by the incident neutron beam [9], leading to uncertainty in what value to use to correct for bending in the neutron data.

In this experiment, we avoid difficulties of this nature by using neutrons to characterize the bending. This is done using neutrons of two almost harmonic wavelengths diffracting off the 220 and 400 lattice planes of the crystal blades and thus following approximately the same paths through the interferometer and illuminating the same regions of each crystal blade. We then exploit the different assumed functional dependencies on the neutron de Broglie wavelength λ of the phase shifts due to gravity (proportional to λ) and bending (inversely proportional to λ) to separate their effects. We have used two interferometers of different geometry in order to separate and identify systematic discrepancies other than the previously known bending correction that are dependent on the interferometer or how it is mounted in the apparatus.

The experimental arrangement is illustrated in Fig. 2. A nearly monochromatic, collimated beam of neutrons is incident upon a neutron interferometer constructed out of a single perfect crystal of silicon. The crystal lattice of the silicon acts as a three-dimensional diffraction grating for neutrons, allowing the various blades of the interferometer to act as mirrors or beam splitters due to Bragg diffraction. A perfect crystal is used to ensure that the lattice planes of the various blades are perfectly aligned. The first blade of the interferometer splits the neutron beam into two components, which are redirected by the intermediate blades to recombine in the final blade. The difference in optical path length and therefore the phase accumulated by the neutron along one path relative to the other can be modified by varying the potential energy of the neutron along the two spatially separated beam paths. These differences in accumulated phase are measured as the swapping of intensity between the two ^{3}He gas proportional detectors $C2$and $C3$. A 2-mm-thick aluminum phase flag is placed across both beams and rotated through the angle labeled δ in Fig. 2 about an axis perpendicular to the scattering plane of the interferometer to produce a phase shift by varying the relative path length that the two beams must travel in aluminum. It is also possible to produce a phase shift by tilting the entire assembly consisting of the interferometer, detectors, and phase flag about the incident beam of neutrons through the angle labeled α in Fig. 2 so that the horizontal portions of the two paths I and II for the neutron are at different heights and thus different gravitational potentials.

The items shown in Fig. 2 are contained in a cadmium covered aluminum box for shielding from stray neutrons and thermal variations. This aluminum box provides an isothermal enclosure for the interferometer. It is mounted on an axle which provides an axis for rotation about the incident beam. This assembly is mounted inside a heavy masonite box that is supported on four pneumatic vibration isolation cylinders and enclosed in a Plexiglas greenhouse for further isolation from thermal variations and airborne microphonic vibrations. The neutron wavelengths for this experiment were selected using a focusing double-crystal monochromator with pressed copper monochromator crystals. A diagram of our experimental apparatus at the University of Missouri Research Reactor (MURR) is shown in Fig. 3.

In order to detect discrepancies that may be related to the interferometer, the experiment was performed using two interferometers of differing geometry. For each interferometer, two different wavelengths of neutrons were used to compensate for bending effects as described below. One interferometer, shown in Fig. 4, is a skew-symmetric interferometer with blade separations $d_1=16.172(3)$ mm and $d_2=49.449(3)$ mm and blade thickness $a=2.621(3)$ mm. The other interferometer, shown in Fig. 5, is a symmetric interferometer similar in geometry to the interferometers used in previous COW experiments but larger in size and therefore more sensitive. It has a separation between blades $d_1=d_2=50.404(3)$ mm and a blade thickness of 3.077(3) mm.

II. THEORETICAL BACKGROUND

The Hamiltonian for the neutron moving in the interferometer's frame of reference on the surface of our rotating Earth is [2]

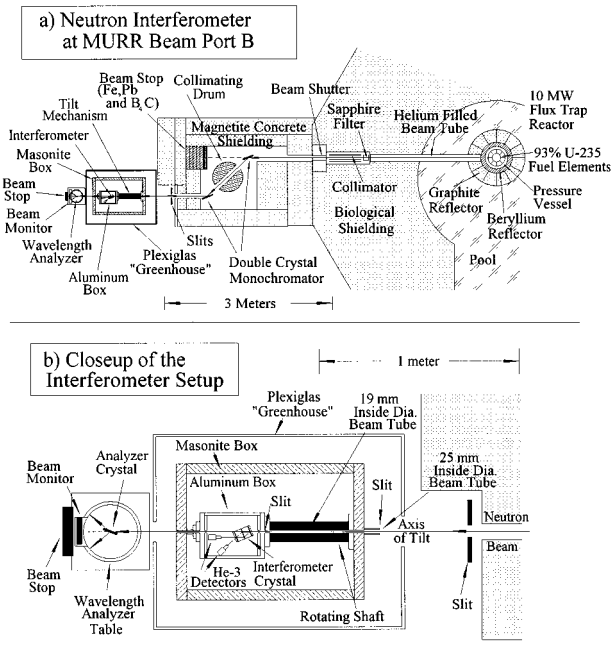

FIG. 3. The beamport *B* neutron interferometry apparatus at MURR: (a) a top view of beamport *B* illustrating the positions of the interferometer and the double crystal monochromator, and (b) a closeup view showing the box within a box vibration isolation arrangement.

$$\mathcal{H}=\frac{|\mathbf{p}|^2}{2m_i}-\frac{GMm_g}{r}-\mathbf{\Omega}\cdot\mathbf{r}\times\mathbf{p}, \tag{1}$$

where G is Newton's universal gravitational constant, m_i and m_g are the inertial and gravitational masses of the neutron, M is the Earth's mass, $\mathbf{\Omega}$ is the Earth's angular velocity of rotation, $\mathbf{r}$ is the neutron's position relative to the Earth's center, and $\mathbf{p}$ is the neutron's canonical momentum. The Lagrangian can be written down using the inverse Legendre transformation

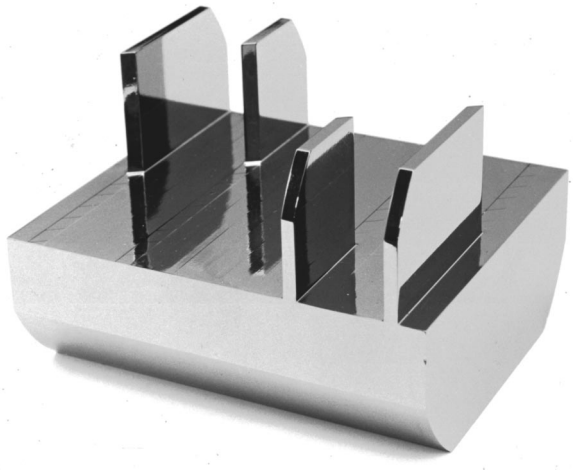

FIG. 4. A photograph of the skew-symmetric interferometer used in this experiment. The dimensions of the interferometer are $d_1=16.172$ mm, $d_2=49.449$ mm, and $a=2.621$ mm. This interferometer was machined in the physics shop at the University of Missouri-Columbia.

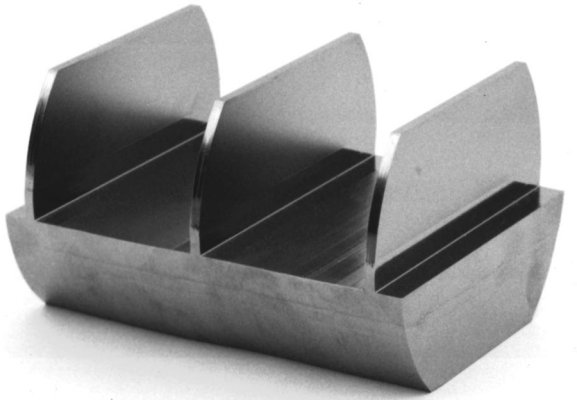

FIG. 5. A photograph of the symmetric interferometer used in this experiment. The blades of the interferometer are 3.077 mm thick and 50.404 mm apart. This interferometer was machined at Atominstitut, Vienna, Austria.

$$\mathcal{L}=\mathbf{p}\cdot\mathbf{v}-\mathcal{H}$$
$$=\frac{1}{2}m_i|\mathbf{v}|^2+\frac{GMm_g}{r}+m_i(\mathbf{\Omega}\times\mathbf{r})\cdot\mathbf{v}+\frac{1}{2}m_i|\mathbf{\Omega}\times\mathbf{r}|^2, \tag{2}$$

where $\mathbf{v}$ is the neutron's velocity relative to the interferometer. The canonical momentum is readily obtained from this Lagrangian,

$$\mathbf{p}=\frac{\partial\mathcal{L}}{\partial\mathbf{v}}=m_i\mathbf{v}+m_i\partial\times\mathbf{r}. \tag{3}$$

Since the interferometer is very small compared to the Earth's radius $\mathbf{R}$, we define a local position variable $\mathbf{x}=\mathbf{r}-\mathbf{R}$, where $\mathbf{R}$ is taken to extend from the center of the Earth to the point at which the neutron enters the interferometer. Thus, to a very good approximation we have

$$\mathcal{L}\cong\tfrac{1}{2}m_i|\dot{\mathbf{x}}|^2+m_g\mathbf{g}\cdot\mathbf{x}+m_i(\mathbf{\Omega}\times\mathbf{x})\cdot\dot{\mathbf{x}}+\mathcal{L}_0, \tag{4}$$

where $\mathcal{L}_0=\mathcal{L}(\mathbf{R})$, the velocity $\mathbf{v}rs=\dot{\mathbf{x}}$, and

$$\mathbf{g}=-\left(\frac{GM}{R^2}\hat{\mathbf{R}}+\frac{m_i}{m_g}\Omega\times(\mathbf{\Omega}\times\mathbf{R})\right) \tag{5}$$

is the effective acceleration due to gravity and the centrifugal force. The magnitude of this effective gravitational acceleration is 9.800 m/s^2 at the surface of the Earth in Columbia, Missouri, as determined from values measured in St. Louis and Kansas City [10]. Although $\mathbf{g}$ contains a component derived from the centrifugal force and thus couples the gravitational and inertial masses, we do not expect this to be a problem in this experiment because it is expected from classical physics to result in a reduction in the magnitude of $\mathbf{g}$ of only 2 parts in 1000 from the value determined by gravity alone.

When the neutron is inside the aluminum phase shifter, the Lagrangian has an additional component due to the neutron-nuclear optical potential U_n related to the strong nuclear force, so that the total Lagrangian inside the aluminum is

$$\mathcal{L} \cong \tfrac{1}{2} m_i |\dot{\mathbf{x}}|^2 + m_g \mathbf{g}\cdot\mathbf{x} + m_i(\boldsymbol{\Omega}\times\mathbf{x})\cdot\dot{\mathbf{x}} - U_n + \mathcal{L}_0, \quad (6)$$

This component is given by

$$U_n = 2\pi\hbar^2 N b/m, \quad (7)$$

where N is the number density of atoms in the aluminum, and b is the average coherent neutron scattering length for the aluminum nuclei. Because of this additional potential energy the aluminum plate of thickness D acts as a phase shifter for the neutron beams in the interferometer.

The effective gravitational, Coriolis, and neutron-nuclear optical potential-energy terms are all small compared to the kinetic energy of the neutrons for all of the wavelengths used so that the quantum-mechanical phase accumulated by a particle in traveling along one path through an interferometer can be calculated semiclassically by integrating the action of the particle along its straight-line, free-particle trajectory in time and space [11]. This method, based on the idea of Feynman-Dirac path integrals [12,13], is accurate to first order in the potential energy for potential energies small relative to the kinetic energy of the free particle. This condition is easily met since $m_g g \approx 1$ meV/cm, $U_n \approx 0.05$ μeV, and $E = m_i v_0^2/2 \approx 20$ meV for $\lambda \approx 2$ Å neutrons. According to this approach, the difference between the phases accumulated along path I and path II, defined by

$$\Delta\Phi \equiv \Phi_{\mathrm{II}} - \Phi_{\mathrm{I}}, \quad (8)$$

is given by

$$\Delta\Phi = \frac{1}{\hbar}\left[\int \mathcal{L}(\mathbf{x}_{\mathrm{II}}(t), \dot{\mathbf{x}}_{\mathrm{II}}(t), t)dt - \int \mathcal{L}(\mathbf{x}_{\mathrm{I}}(t), \dot{\mathbf{x}}_{\mathrm{I}}(t), t)dt\right], \quad (9)$$

where $\mathbf{x}_{\mathrm{I}}(t)$ and $\mathbf{x}_{\mathrm{II}}(t)$ are the positions of the particle as a function of time along the free-particle trajectories of paths I and II, respectively. Since the Lagrangian in this situation is time dependent, Eq. (9) can be reduced to

$$\Delta\Phi = \frac{1}{\hbar}\left[\int_{\text{path II}} \mathbf{p}\cdot\mathbf{dl} - \int_{\text{path I}} \mathbf{p}\cdot\mathbf{dl}\right] \quad (10)$$

by use of the inverse Legendre transformation, Eq. (2). The locally defined canonical momentum is given by

$$\mathbf{p} \cong m_i\left(v_0 - \frac{m_g \mathbf{g}\cdot\mathbf{x}}{m_i v_0}\right)\hat{\boldsymbol{l}} + m_i \boldsymbol{\Omega}\times\mathbf{x} \quad (11)$$

outside the phase shifter, and

$$\mathbf{p} \cong m_i\left(v_0 - \frac{m_g \mathbf{g}\cdot\mathbf{x}}{m_i v_0} - \frac{U_n}{m_i v_0}\right)\hat{\boldsymbol{l}} + m\Omega\times\mathbf{x} \quad (12)$$

inside, where $\hat{\boldsymbol{l}}$ is the unit vector along the trajectory of the neutron and $v_0 = 2\pi\hbar/m\lambda$ is the initial speed of the neutron when it enters the interferometer. In this form the phase shifts due to the effects of gravity, rotation, and the phase shifter can be calculated independently.

Since the incident beam is level, gravity and the centrifugal force due to the Earth's rotation result in a phase shift of

$$\Delta\Phi_{\mathrm{grav}} = \frac{m_g}{\hbar v}\left[\int_{\text{path II}} \mathbf{g}\cdot\mathbf{x}\, dl - \int_{\text{path I}} \mathbf{g}\cdot\mathbf{x}\, dl\right]$$
$$= -m_g g A_0 \sin\alpha/\hbar v_0 = -2\pi\lambda m_i m_g \frac{g}{h^2} A_0 \sin\alpha, \quad (13)$$

where

$$A_0 = [2d_1 d_2 + a(d_1 + d_2)]\tan\theta_B \quad (14)$$

is the area enclosed by the trajectories of the neutrons (see Fig. 2) that exactly satisfy the Bragg condition along the two paths of the interferometer assuming no deflections due to potentials other than that of the interferometer itself. Equation (14) is the area for the skew-symmetric interferometer, with Bragg angle θ_B. For the symmetric interferometer $d_1 = d_2$. Thus, the phase shift due to gravity can be written in the form

$$\Delta\Phi_{\mathrm{grav}}(\alpha,\lambda) = -u\lambda \sin\alpha \tan\theta_B, \quad (15)$$

where the wavelength-independent parameter

$$u \equiv \frac{m_i m_g g A_0}{2\pi\hbar^2 \tan\theta_B}. \quad (16)$$

Note that $A_0/\tan\theta_B$ depends only on the blade thickness a and their separations d_1 and d_2. The calculated value of the parameter u is 69.695(16) rad/Å for our skew-symmetric interferometer and 212.119(21) rad/Å for our large symmetric interferometer.

Since the experiment is done in the Earth's rotating frame of reference, the Coriolis force on the moving neutron gives rise to a phase shift known as the Sagnac or Page effect [14–16]. It is given by

$$\Delta\Phi_{\mathrm{Sagnac}}(\alpha,\lambda) = \frac{m_i}{\hbar}\boldsymbol{\Omega}\cdot\left[\int_{\text{path II}} \mathbf{x}\times\mathbf{dl} - \int_{\text{path I}} \mathbf{x}\times\mathbf{dl}\right]$$
$$= \frac{m_i}{\hbar}\oint (\boldsymbol{\Omega}\times\mathbf{x})\cdot\mathbf{dl}$$
$$= 2m_i\boldsymbol{\Omega}\cdot\mathbf{A}_0/\hbar, \quad (17)$$

where $\mathbf{A}_0$ is the normal area vector corresponding to the loop in space whereby the neutron leaves the source along path II and returns to it via path I. Since the beam incident on the interferometer is oriented from North to South and is level with respect to gravity, the Sagnac phase shift for our experiment is

$$\Delta\Phi_{\mathrm{Sagnac}} = -s \cos\alpha \tan\theta_B. \quad (18)$$

The factor s is given by

$$s \equiv \frac{2m_i\Omega A_0 \cos\theta_L}{\hbar \tan\theta_B}, \quad (19)$$

where $\theta_L = 51.37°$ is the colatitude angle for Columbia, Missouri. The value of s is 2.5616(6) rad for the skew-

symmetric interferometer and 7.7962(7) rad for the symmetric interferometer and is independent of wavelength.

The phase shift due to the aluminum phase shifter is determined by the difference in the relative thickness of aluminum along the two paths. From the geometry of our experiment this nuclear phase shift is

$$\Delta\Phi_{\mathrm{nuc}}(\delta,\lambda)=\lambda NbD\left[\frac{1}{\cos(\theta_B+\delta)}-\frac{1}{\cos(\theta_B-\delta)}\right], \tag{20}$$

where D is the thickness of the phase shifter and δ is the angle through which it is rotated defined as shown in Fig. 2.

The interferometers are inevitably somewhat strained as a result of the process of machining with diamond cutting wheels, even after etching, and the way in which they are mounted in the apparatus. They can also deform under their own weight when tilted. Deformation of interferometers sufficient to cause significant phase shifts has been observed experimentally in previous experiments and also modeled by mathematical simulation for a symmetric interferometer [17]. Although the bending predicted by simulation is quite complicated and that of the actual interferometer is expected to be even more so, we have assumed for the purpose of our analysis of the experiment that the only effects of bending and strains on the phase are the result of a slightly longer free-space path length in one path of the interferometer than in the other. This produces a phase shift of

$$\Delta\Phi_{\mathrm{bend}}(\alpha,\lambda)=2\pi\lambda^{-1}\Delta\not{\ell}(\alpha), \tag{21}$$

where $\Delta\not{\ell}(\alpha)$ is the amount that path II is longer than path I due to bending. The x-ray experiments of Staudenmann *et al.* [2] using a small, symmetric interferometer have shown empirically that this phase difference can be modeled by

$$\Delta\Phi_{\mathrm{bend}}=w\lambda^{-1}\sin\alpha\,\sin^2\theta_B, \tag{22}$$

where the factor w is dependent on the interferometer used and the way in which it is mounted in the apparatus, but independent of wavelength λ. While the axes of symmetry for mechanical stress of a skew-symmetric interferometer are very different, we have assumed that the functional form of the bending correction remains the same. For the purpose of analysis of this experiment, we have assumed that the bending and strains of the interferometer have no other effects, a point that we shall return to later.

Although the theoretical treatment so far has assumed an incident plane wave, the incident beam is neither perfectly collimated nor perfectly monochromatic. Due to the geometry of the monochromator, there is a distribution of angles between the trajectories of the neutrons in the vertical plane. Since the monochromator uses pressed copper crystals, there is also a distribution of wavelengths reflected in any given direction and a distribution of angles in the scattering plane of the interferometer at which neutrons satisfy the Bragg condition. These distributions produce variations in exit beam intensity and influence visibility of fringes and the frequency of oscillations as functions of tilt angle due to interference and coherence effects as discussed below.

Since there is a distribution of velocities of neutrons incident on the interferometer in any given direction, there is a distribution in the degree to which these neutrons fail to satisfy the exact Bragg condition. As first discussed by Petrascheck *et al.* [18], neutrons that do not satisfy the exact Bragg condition can take sixteen different paths through the interferometer from a single point on the entrance blade due to dynamical diffraction. These paths are shown for a skew-symmetric interferometer in Fig. 6. Horne [19] has pointed out that these paths form multiple interacting interferometers and proposed a solution in integral form for a symmetric Laue interferometer. The integrals have been worked out analytically by Werner *et al.* [16] for the beam accepted by the $C3$ detector using a symmetric interferometer assuming equal probability for all velocities, an assumption that is justified by the fact that the distribution of velocities accepted by the interferometer as determined by the Darwin width is very small compared to the incident distribution of velocities. This analysis has recently been generalized [20] to include skew-symmetric interferometers and extended to describe interference and diffraction effects observed by the $C2$ detector and occurring along each average path I and II for both detectors with the other path blocked. Independently, Bonse and Wroblewski [21] have shown that similar corrections to the phase due to dynamical diffraction effects are significant in a related experiment involving an accelerated interferometer. Corrections of this sort require the phase shift due to gravity to be scaled by a factor $[1+\varepsilon(\alpha,\lambda)]$ and cause the mean intensity and visibility of the fringes also to vary as functions of the tilt angle, wavelength, and parameters of the interferometer due to this averaging over the incident velocity of neutrons in a given interference pattern.

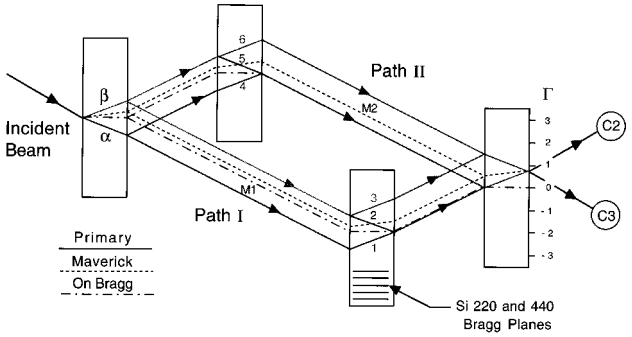

FIG. 6. A diagram of eight of the possible paths through the interferometer predicted by dynamical diffraction theory. The six primary paths (solid lines) interfere with each other as do the two maverick paths (dashed lines), but the primary paths do not interfere coherently with the maverick paths as they arise from different components of the incident beam. Another eight paths exit at the same point on the final blade of the interferometer for negative values of the entrant Γ.

Since each component of the incident beam satisfying a different Bragg angle feels a different phase shift due to both gravity and the Sagnac effect, the components dephase causing a tilt-dependent loss of contrast. This is analogous in some ways to the loss of contrast due to larger amounts of matter in one path of the interferometer that is observed in longitudinal coherence length and phase echo experiments [22–24]. Assuming that the distribution of intensity in the incident beam at angles in the scattering plane for which the Bragg condition is exactly satisfied is given by

$$P(\theta)=\frac{1}{\sqrt{2\pi}\sigma_\theta}\exp\left(-\frac{(\theta-\theta_B)^2}{2\sigma_\theta^2}\right). \tag{23}$$

This effect requires that the amplitude of oscillation be scaled by the dephasing factor

$$C(\alpha,\lambda)=\exp\left(-\frac{2[\Delta\Phi_{\rm grav}(\alpha,\lambda)+\Delta\Phi_{\rm Sagnac}(\alpha,\lambda)]^2\sigma_\theta^2}{\sin^2 2\theta_B(\lambda)}\right), \tag{24}$$

where σ_θ is estimated to be about 6 mrad from the widths of the peaks in wavelength determination scans. The effect of this angular dispersion on the measured average phase is negligible.

The contrast of a measured interferogram can be less than the theoretical ideal maximum for a variety of reasons including vibration, strains, and surface irregularities of the interferometer blades. Vibrations of the interferometer can be treated as the result of rotations that are randomly distributed in angular frequency and axis of rotation. The time averaging of the Sagnac phase shifts due to rotational noise results in a loss of visibility that is proportional to the interferometer area. The presence of a Moiré pattern due to strains in the interferometer or imperfections in its manufacture will also produce a loss of visibility. Since strain in the crystal and thus the interference fringe pattern may change as the interferometer is tilted, this effect also may be tilt dependent.

III. EXPERIMENTAL RESULTS

A. Tilt-angle interferograms

Samples of interferograms measured by rotating the interferometer tilt α with the phase flag fixed for both wavelengths in both interferometers are shown in Figs. 7 and 8. Note that the point of maximum contrast is different for each situation. The fact that the point of maximum visibility in the actual data is not at zero tilt indicates that strains may be present in the interferometer even when it is level. Also, the sum of the intensities in the detectors $C2$ and $C3$ is not constant but is a function of tilt angle α. This is the result of the variation in intensity of neutrons accepted by the interferometer due to the tilt of the scattering plane of the interferometer relative to that of the monochromator as discussed by Werner *et al.* [25]. We compensate for this variation by normalizing the intensity measured in each detector to the sum of the intensities measured in both detectors $C2$ and $C3$ at each value of α. The normalized $C2$ and $C3$ tilt-angle interferograms for the longer wavelength used with the symmetry interferometer are shown in Fig. 9. The maximum fringe visibility in the $C3$ interferogram is about 60%. The intensities at the maxima of the interferograms decrease more slowly than the intensities at the minima increase as we move away from zero tilt. Furthermore, the frequency of oscillation of intensity is reduced away from the central region. For large values of the tilt angle no interference fringes are visible.

The theoretical normalized interferograms in Fig. 10 show our present understanding of the situation. Figure 10(a) shows the results of including the effects of dynamical diffraction. This interferogram exhibits the reduction of amplitude and frequency of oscillation away from zero tilt. These features are the result of the averaging of the interference patterns produced by neutrons traversing all of the paths through the interferometer that are possible if the Bragg condition is not exactly satisfied. Although the dynamical diffraction effects explain some features of the observed data, the theory predicts a partial recovery of visibility at large values of α that is not observed experimentally. Including the coherence length effects due to averaging over the different wavelengths that satisfy the Bragg condition prevents this recovery of visibility as shown in Fig. 10(b). If the visibility of the interference fringes is scaled to match the observed visibility at zero tilt without adjusting the mean as shown in Fig. 10(c), the difference between the rates of decrease of the intensity maxima and increase of the minima in the central region of the interferogram is better reproduced. This envelope shape occurs due to interference among the sub-beams of the interferometer that comprise path I and path II resulting in a minimum in the mean intensity at $\alpha=0$.

While we have explained several features of the tilt angle interferograms qualitatively, quantitative difficulties remain. In the central region the intensity maxima are more constant than expected and theory appears to overestimate the rate at which both the amplitude and the mean of the interferogram change as a function of α. The discrepancies between data and theory in the ratios of the means of the two detectors at various tilt angles may be a result of failure to adjust the data to compensate for the background counting rates in the two detectors, which may also be a (weak) function of the tilt.

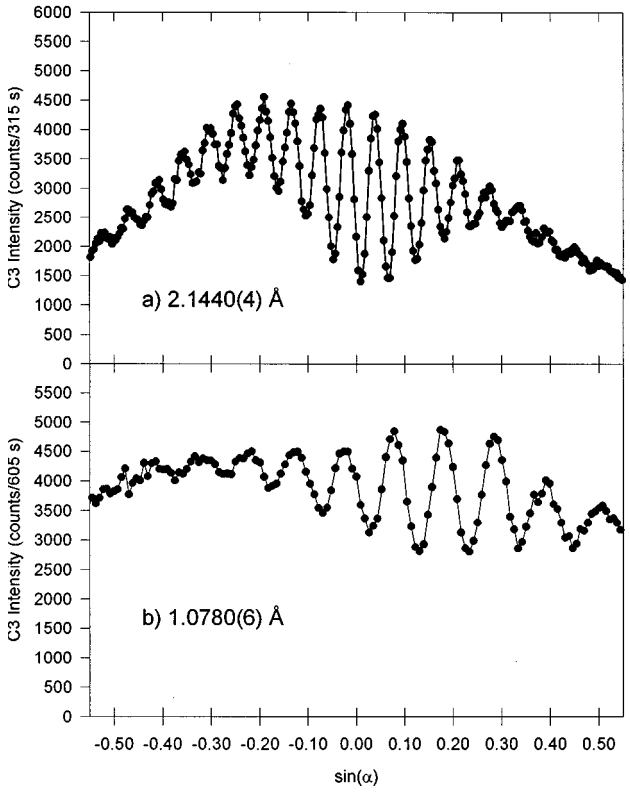

FIG. 7. Gravity interferograms observed in the $C3$ detector produced at the wavelengths (a) 2.1440 Å and (b) 1.0780 Å using the skew-symmetric interferometer.

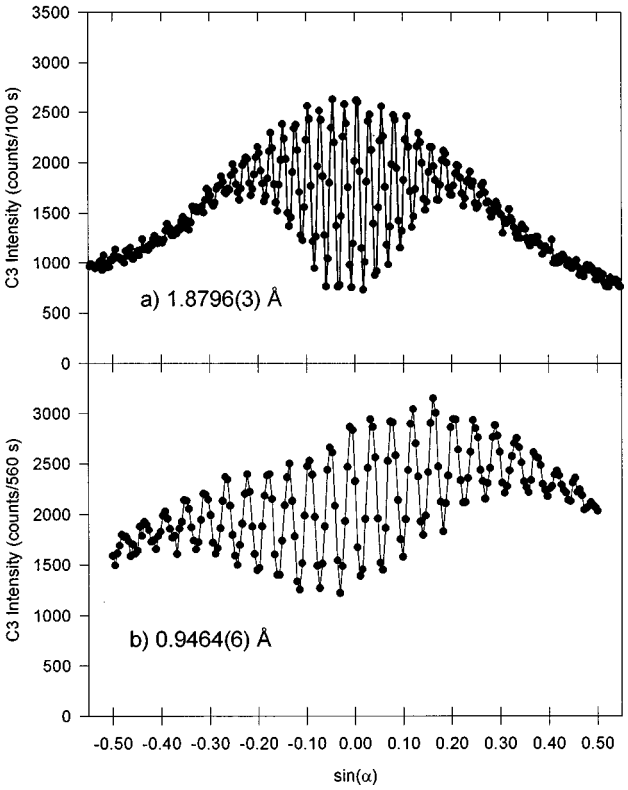

FIG. 8. Gravity interferograms observed in the $C3$ detector produced at the wavelengths (a) 1.8796 Å and (b) 0.9464 Å using the symmetric interferometer by varying the interferometer tilt angle α with the aluminum phase flag fixed.

B. Wavelength measurement and selection

The wavelength of neutrons used in this experiment was set by adjusting the angles of two copper crystals in the double-crystal monochromator. The wavelengths were selected for each of the interferometers so that contrast at the long wavelength for each interferometer was as high as possible and the second-harmonic wavelength was accessible to the monochromator. The shorter, second-harmonic wavelength was chosen by adjusting the angles of the monochromator crystals until the centers of peaks measured by varying the angle of the normal to the 220 (and thus 440) lattice planes of the interferometer relative to the incident beam nearly coincide as shown in Fig. 11.

In this experiment, the wavelength of the neutrons participating in the interference was measured using the experimental arrangement shown in Fig. 12. A pyrolytic graphite (PG) crystal with the 002 planes nominally parallel to its surface was attached to a shaft perpendicular to the scattering plane of the interferometer in path II of the interferometer while path I is blocked by a small piece of shielding made of B_4C in epoxy resin. Determination of each wavelength used was done by measuring the separation between the minima of the sum of the intensities in the $C2$ and $C3$ detectors as the PG crystal was rotated through the first- and second-order Bragg reflections and averaging the results of several high-resolution, long counting time scans such as those shown in Fig. 13. The mean wavelengths of the neutrons used with the skew-symmetric interferometer were found to be $\lambda_2=2.1440(4)$ Å and $\lambda_1=1.0780(6)$ Å, corresponding to

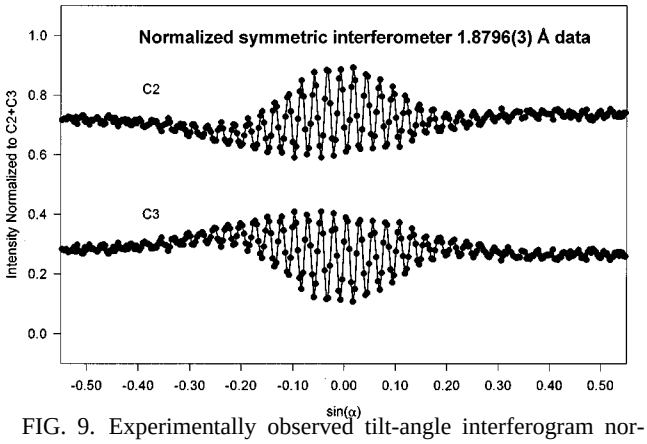

FIG. 9. Experimentally observed tilt-angle interferogram normalized to $C2+C3$ to compensate for the dependence on tilt of the intensity of neutrons accepted by the interferometer for 1.8796-Å neutrons in the symmetric interferometer.

Bragg angles of $\theta_{2B}=33.94°$ and $\theta_{1B}=34.15°$ with respect to the Si [220] and [440] planes, respectively. Those used with the symmetric interferometer were $\lambda_2=1.8796(3)$ Å and $\lambda_1=0.9464(6)$ Å with the corresponding Bragg angles $\theta_{2B}=29.304°$ and $\theta_{1B}=29.504°$.

After completion of the experimental runs for each interferometer a high-resolution scan was repeated for each wavelength to verify that the wavelengths used had not changed

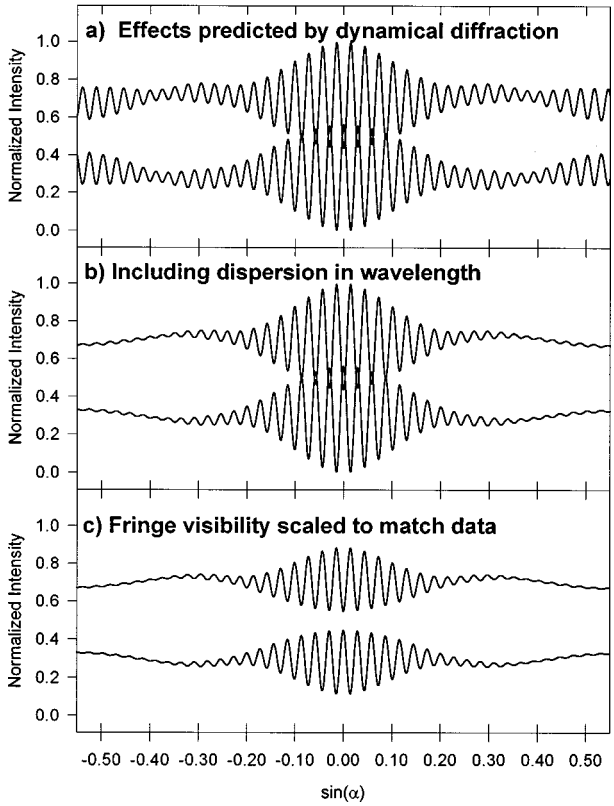

FIG. 10. Theoretically predicted tilt-angle interferograms normalized to $C2+C3$ for 1.8796-Å neutrons in the symmetric interferometer (a) as predicted by the dynamical theory of diffraction, (b) modified to include the reduction in visibility as the interferometer is tilted due to wavelength dispersion, and (c) scaled to match the visibility of the observed interferogram at $\alpha=0$.

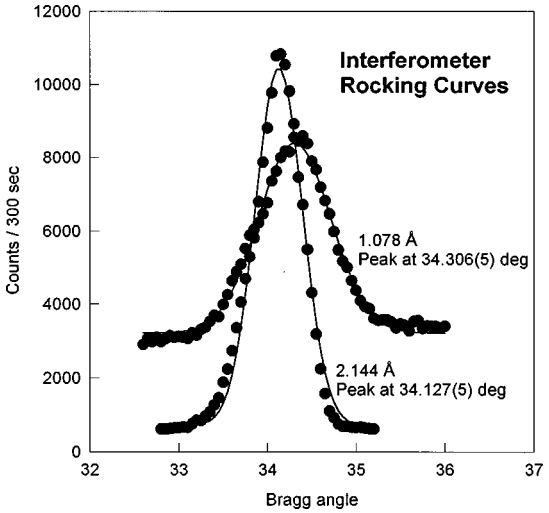

FIG. 11. Interferometer rocking curve scans for the skew-symmetric interferometer. Note the near coincidence of the Bragg peaks for the two wavelengths.

during the course of the experiment. The wavelengths determined before and after the experimental run were found to be in agreement to within the uncertainties quoted above. We also tested for any dependence of the measured wavelength on the tilt of the interferometer by performing wavelength measurement scans at various values of α. Again, the values measured in these scans are in statistical agreement with those measured at $\alpha=0°$.

C. Phase-shifter interferograms

Since interferograms of the type shown in Figs. 7, 8, and 9, referred to as ''tilt-angle interferograms,'' vary in both amplitude and frequency of oscillation over the range of tilt

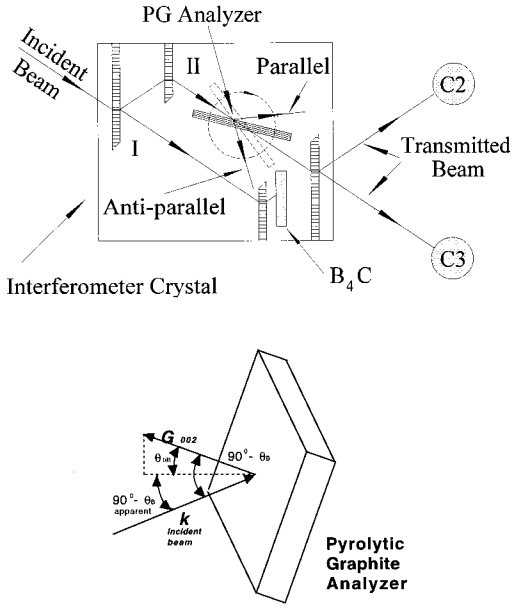

FIG. 12. A diagram of the experimental arrangement for wavelength determination. A pyrolitic graphite crystal is rotated in one subbeam of the interferometer with the other blocked. The PG crystal may also be tilted vertically with respect to the incident beam to ensure a horizontal scattering plane as shown in the lower diagram.

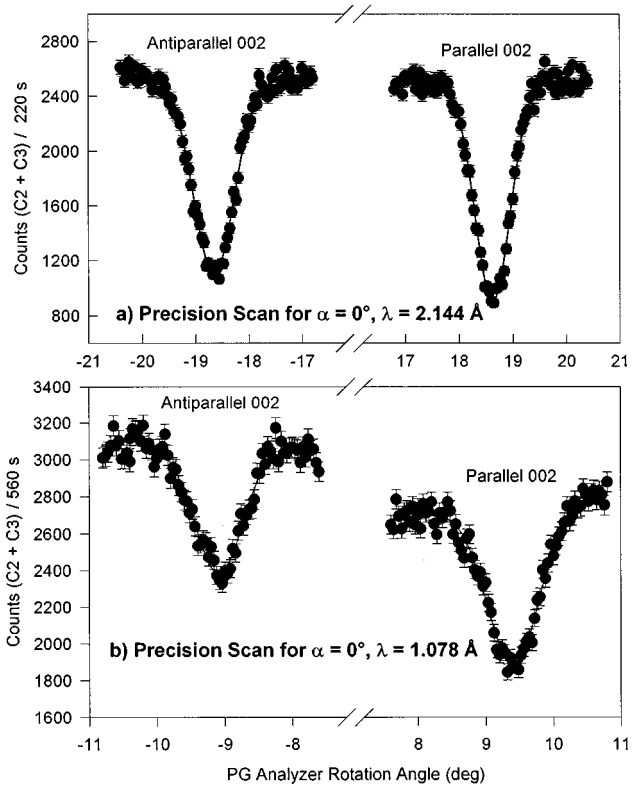

FIG. 13. Precision PG analyzer scans used for wavelength determination for the skew-symmetric interferometer. The scans were conducted using a vertical analyzer scanned across the parallel and anti-parallel graphite 002 Bragg peaks. The peaks were least-squares fitted assuming a Gaussian (with a linear background subtracted).

angle scanned in a complicated fashion that is known only qualitatively, it is difficult to use them to study phase shifts in a precise, quantitative fashion. For quantitative measurement of the phase shift due to gravity we generate interferograms at various tilt angles α for each neutron wavelength separately by rotating the aluminum phase shifter. The intensity measured by interferograms of this type, referred to as ''phase-shifter interferograms,'' is described by a function derived from Eq. (20), which we write as

$$I(\delta,\alpha)=a+b\,\cos\left[\omega\left(\frac{1}{\cos(\theta_B+\delta_0+\delta)}-\frac{1}{\cos(\theta_B-\delta_0-\delta)}\right)+\Delta\Phi(\alpha,\lambda)\right], \tag{25}$$

which can be fit using nonlinear least-squares methods to extract the offset phase $\Delta\Phi(\alpha,\lambda)$ containing the gravitational phase shift. The interferogram oscillation frequency ω and the offset rotation angle δ_0 are initially allowed to vary as parameters of the fit. After a large number of scans, the fitted values for ω and δ_0 are averaged for each interferometer to obtain the fixed values used in the final analysis, leaving only 3 adjustable parameters, a, b, and $\Delta\Phi(\alpha\lambda)$.

The series of interferograms shown in Fig. 14 demonstrates that the phase of the interferograms advances about twice as fast with the tilt angle α for the longer wavelengths as for the shorter ones as predicted by Eq. (15). The inter-

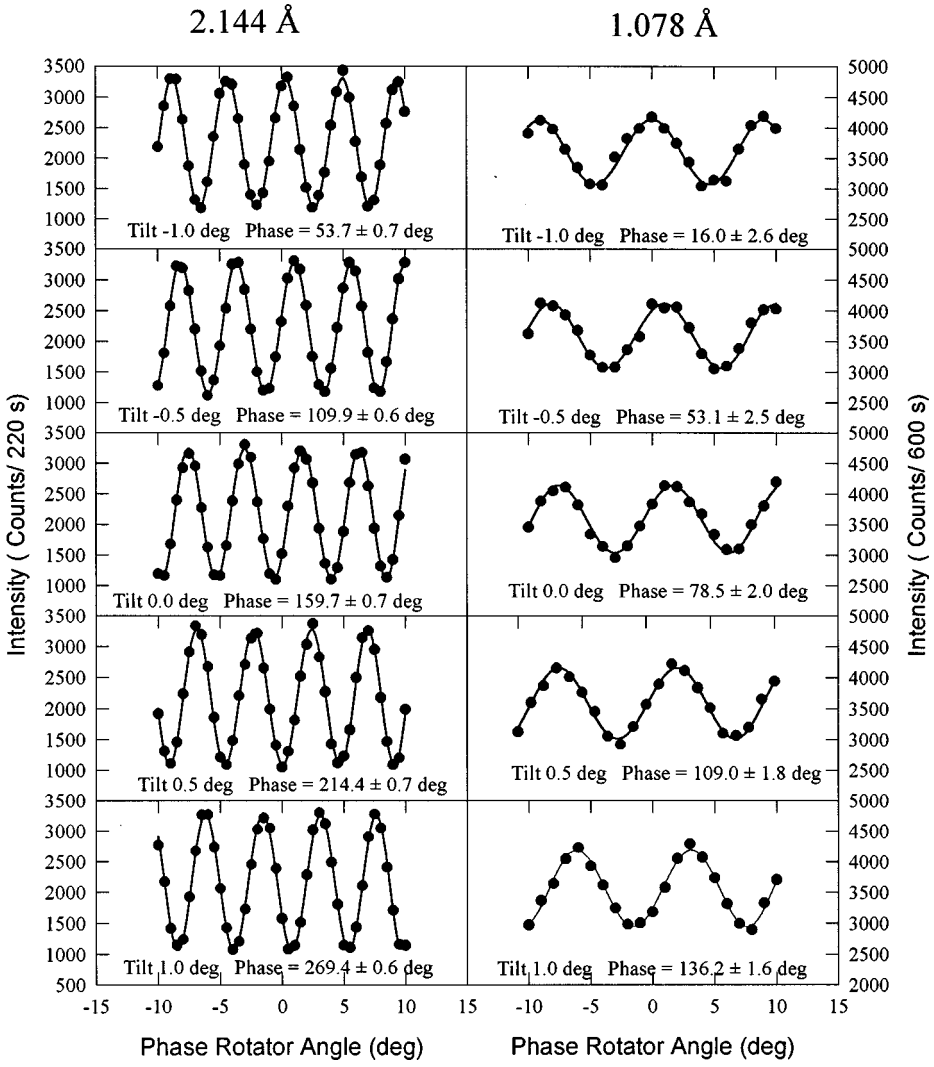

FIG. 14. A series of phase rotator scans taken for various values of α using the wavelengths (a) 2.1440 Å and (b) 1.0780 Å in the skew-symmetric interferometer. The phase advances almost the same amount with each step and nearly twice as much for the 2.1440-Å data as for the 1.0780-Å data.

ferograms generated at various tilt angles for each wavelength were sequentially interleaved with ones measured with the interferometer level. By comparing the phase of the ones measured at a given tilt angle with the average of the phases of the level interferometer measurements immediately preceding and following it, we are able to compensate for small drifts in the baseline phase of the interferometer. This method also minimizes the effects of the phase shift due to the Sagnac effect to a large extent. By subtracting the zero-tilt Sagnac phase shift from the data, the Sagnac phase shift in the adjusted data is described by the difference expression

$$\Delta\Phi_{\text{Sagnac}} = s\ \tan\theta_B(1-\cos\alpha), \tag{26}$$

which is very small for the useful range of tilt angles. Previous measurements of the neutron Sagnac phase shift [2,26,27] have shown agreement between experiment and theory on the order of a few percent. Since this phase shift is sufficiently small compared to that due to gravity it can be treated as a known quantity to the resolution of this experiment. We compensate for it by subtracting the calculated value from the raw data for each wavelength at each tilt setting. The phase shift data with the Sagnac phase removed is shown in Fig. 15, illustrating that the agreement between the data and the theoretical phase shift due to gravity is better for the longer of the two wavelengths for both interferometers used.

IV. PHASE-SHIFT DATA ANALYSIS

The total phase shift $\Delta\Phi(\alpha,\lambda)$ obtained from fitting the phase-shifter interferograms is composed of three terms

$$\Delta\Phi(\alpha,\lambda) = \Delta\Phi_{\text{grav}}(\alpha,\lambda) + \Delta\Phi_{\text{bend}}(\alpha,\lambda) + \Delta\Phi_{\text{Sagnac}}(\alpha,\lambda), \tag{27}$$

where we assume that the functional form of each term on the tilt angle α and the wavelength λ as described above is correct. Thus, we use the equation

$$\Delta\Phi(\alpha,\lambda) = -(u\lambda\ \sin\alpha)F_g(\alpha,\lambda) + (w\lambda^{-1}\ \sin\alpha)F_b(\lambda) + s(1-\cos\alpha)\tan\theta_B \tag{28}$$

to determine the parameters u and w from the phase-shift data. The functions F_g and F_b are

$$F_g(\alpha,\lambda) = \tan\theta_B[1+\varepsilon(\alpha,\lambda)] \tag{29}$$

and

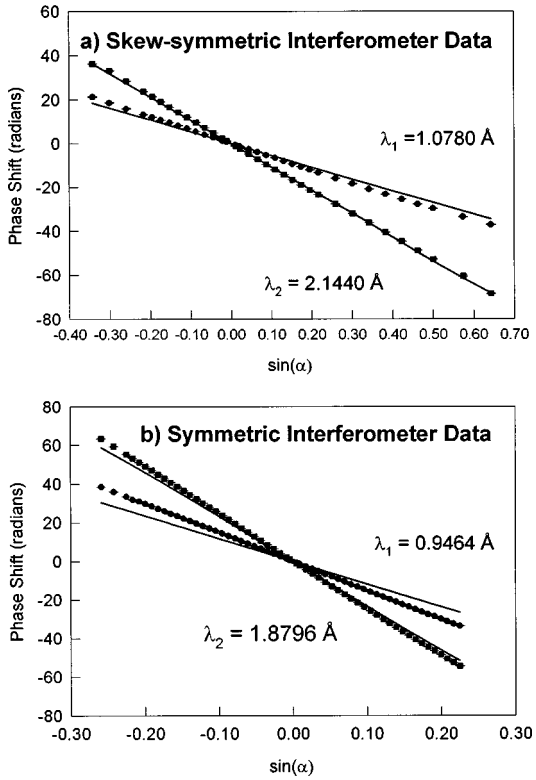

FIG. 15. Graphical representation of the phase shift data using (a) the skew-symmetric interferometer and (b) the symmetric interferometer with the Sagnac effect phase shift subtracted. The solid curves are the gravity phase shifts expected from theory.

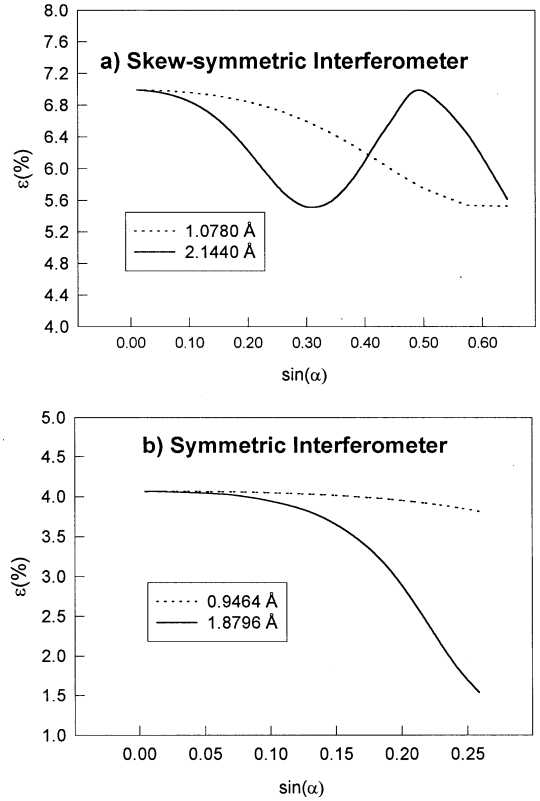

FIG. 16. A plot of the values for the multiple-path dynamical diffraction correction term $\varepsilon(\alpha,\lambda)$ for (a) 2.1440-Å neutrons in the skew-symmetric interferometer and (b) 1.8796-Å neutrons in the symmetric interferometer.

$$F_b(\lambda)=\sin^2\theta_B\,. \tag{30}$$

Calculated values of the multiple-path dynamical diffraction correction factor $\varepsilon(\alpha,\lambda)$ for both interferometers for the longer wavelength used are shown in Fig. 16. This factor is dependent on the interferometer blade thickness a and their separations d_1 and d_2 and on wavelength and tilt as a function with argument $\lambda\sin\alpha$. Since the Sagnac effect phase shift is small relative to the gravitational phase shift and known to sufficient accuracy, we treat it as a known quantity for the purpose of our data analysis and subtract a calculated value of it from the measured phase shift $\Delta\Phi(\alpha,\lambda)$ before fitting the data.

Since we have measured the phase shift $\Delta\Phi$ at two wavelengths λ_1 and λ_2 for each tilt angle α, we have two equations for the two unknown parameters u and w. Theoretically, these parameters should be independent of α and λ. The experimentally determined u and w parameters are then given by

$$u_{\text{expt}}=\frac{\Delta\Phi(\alpha,\lambda_1)\lambda_1F_b(\lambda_2)-\Delta\Phi(\alpha,\lambda_2)\lambda_2F_b(\lambda_1)}{[\lambda_2^2F_g(\alpha,\lambda_2)F_b(\lambda_1)-\lambda_1^2F_g(\alpha,\lambda_1)F_b(\lambda_2)]\sin\alpha} \tag{31}$$

and

$$w_{\text{expt}}=\frac{\Delta\Phi(\alpha,\lambda_1)\lambda_2F_g(\alpha,\lambda_2)-\Delta\Phi(\alpha,\lambda_2)\lambda_1F_g(\alpha,\lambda_1)}{[(\lambda_2/\lambda_1)F_g(\alpha,\lambda_2)F_b(\lambda_1)-(\lambda_1/\lambda_2)F_g(\alpha,\lambda_1)F_b(\lambda_2)]\sin\alpha}. \tag{32}$$

Note that the value of the gravity parameter u_{expt} as determined by Eq. (31) is independent of the assumed functional form of the dependence of $\Delta\Phi_{\text{bend}}(\alpha,\lambda)$on the tilt angle α.

In this manner, we have determined that u_{expt} is 68.63(8) rad/Å for the skew-symmetric interferometer and 210.28(23) rad/Å for the symmetric interferometer. In this analysis, the angular range considered was restricted to $|\alpha|\leqslant 11.25°$ for the skew-symmetric interferometer and $|\alpha|\leqslant 10.00°$ for the symmetric interferometer due to concerns about uncertainties due to loss of fringe visibility. If data taken over the full range of tilt angles used are considered, the values of u_{expt} for the two interferometers become 67.63(22) and 210.82(29) rad/Å. The measured values of u_{expt} at various tilt angles are shown in Fig. 17. Likewise, we have used Eq. (32) to obtain the values

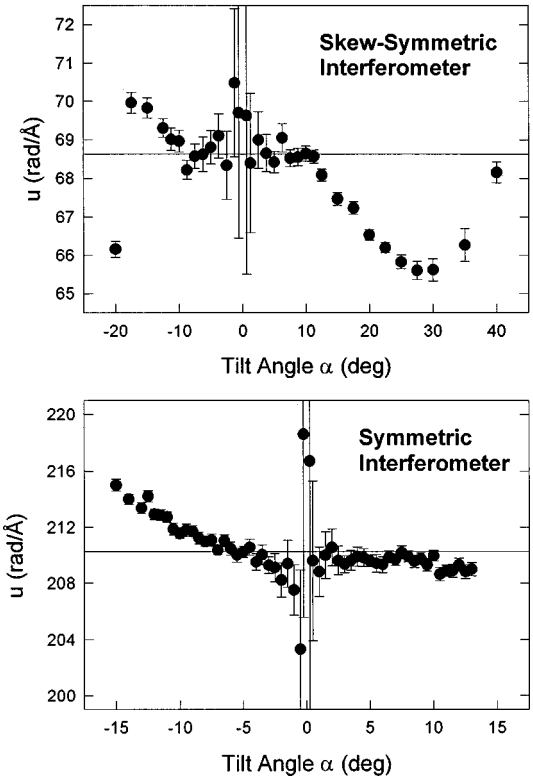

FIG. 17. A plot of the values for the gravitational parameter u experimentally determined pointwise using (a) the skew-symmetric interferometer and (b) the symmetric interferometer. The two horizontal lines are 68.63(8) rad/Å and 210.28(23) rad/Å, the weighted average of the data in the restricted regions of α described in the text.

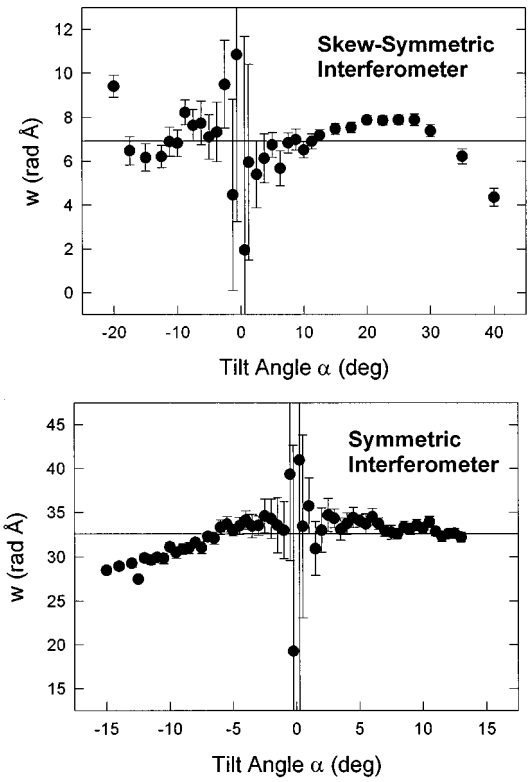

FIG. 18. A plot of the values for the bending parameter w experimentally determined pointwise using (a) the skew-symmetric interferometer and (b) the symmetric interferometer. The two horizontal lines are 6.92(13) rad/Å and 32.61(18) rad/Å, the weighted average of the data in the restricted regions of α described in the text.

of the bending parameter w_{expt} of 6.92(13) rad/Å for the skew-symmetric interferometer and 32.61(18) rad/Å for the symmetric interferometer for the restricted range of tilt angles and 7.34(14) rad/Å and 31.57(25) rad/Å for the full range. The results of the pointwise calculation of w_{expt} are shown in Fig. 18. These results are compared with the theoretical predictions in Table I.

V. DISCUSSION

We have also considered the possible effects due to the incident beam being neither perfectly level nor perfectly horizontally collimated. If the incident beam were out of the horizontal plane by an angle ξ, then the α-dependent gravitational phase shift would be reduced by $\cos(\xi)$ and there would be an additional, constant phase shift that would be removed by our difference method. Similarly, if the interferometer were tilted so that the incident beam formed an angle ξ with its horizonal surface then the size of the gravity-induced phase shift will be increased by $1/\cos^2(\xi)$ by the increase in the effective thickness and separation of the interferometer blades. Since the incident beam and the interferometer are level along the longitudinal direction to less than half a degree, these effects would be negligible. Likewise, the effects on both phase and contrast of a spread in the direction of the incident beam relative to the horizontal surface of the interferometer will be negligible. In these estimates we assumed that the angle of scattering vector of the interferometer was unchanged relative to the incident beam during tilting.

The effects of misalignment between the crystal planes and the macroscopic surface of the interferometer have also been considered. The condition described as level in this work is determined by the use of a spirit level with a precision of 0.1° placed on a surface parallel to the surface of the

TABLE I. Summary of the theoretical and experimental results for the gravity parameter u and estimates of the size of the bending parameter w.

	Skew-symmetric interferometer	Symmetric interferometer
Gravity parameter u Theoretical (rad/Å)	69.695(16)	212.119(21)
Gravity parameter u_{expt} α range restricted (rad/Å)	68.63(8)	210.28(23)
Gravity parameter u_{expt} full range of α(rad/Å)	67.63(22)	210.82(29)
Bending parameter w_{expt} α range restricted(rad/Å)	6.92(13)	32.61(18)
Bending parameter w_{expt} Full range of α (rad/Å)	7.34(14)	31.57(25)

interferometer. The alignment of the crystal planes with respect to the surface of the skew-symmetric interferometer was examined on a double-axis x-ray spectrometer at National Institute of Standards and Technology and found to be parallel to within 0.5°. The situation is expected to be similar for the symmetric interferometer. The only misalignment that has any effect on the result is a tilt of the scattering plane relative to the top surface of the interferometer. This leads to an offset in the measured value of the tilt angle α. An assumed uncertainty in this offset tilt angle of 0.5° introduces a relative uncertainty of 0.1% into the measured value of u, an effect that has been included in the analysis. The measured misalignment is taken into account in the results presented.

The differences shown in Table I between the observed experimental values of the gravity parameter and the calculated theoretical values are significant. The most likely explanation for this discrepancy is that the way in which the effects of strains and bending of the interferometer have been modeled is too naive. In addition to producing a path length difference, bending and strain can cause local variations in the lattice spacing due to stretching or compression and misalignment of the crystal planes on one blade of the interferometer relative to the others. Therefore, it is quite possible that coupling between the bending and effects due to dynamical diffraction is not as small as has been assumed. Although the dimensional changes to the interferometer due to bending are trivially small compared to the area of the interferometer and the areas appearing in the dynamical diffraction correction, the resulting variation of the relative angles of the crystal planes of the interferometer blades may be nontrivial compared with the Darwin width. This would have the result that neutrons perfectly on Bragg in one crystal would be off Bragg slightly in another, introducing additional changes into both the amplitude and phase of the interferogram not seen in the uncoupled dynamical diffraction approach.

There is evidence to support this conclusion in the data. For the skew-symmetric interferometer the agreement of the data with the theoretical phase shift due to gravity after adjusting for bending is much better in the restricted range of α as can be seen from Fig. 19. Also the qualitative agreement between the experimental and theoretical gravity interferograms is better and the tilt angle for which the visibility is maximum is closer to zero for the longer wavelength data. This is to be expected as the parameter

$$y=\frac{2\mathbf{k}\cdot\mathbf{G}+\mathbf{G}\cdot\mathbf{G}}{4m|V_{\mathbf{G}}|/\hbar^2}=\frac{\Delta\theta\Lambda_0}{d_{hkl}}, \tag{33}$$

which is used to characterize the deviation $\Delta\theta$ from the exact Bragg condition and determines the paths along which a particular neutron travels through the interferometer, is proportional to both the neutron wave vector $\mathbf{k}$ and the reciprocal lattice vector for the diffracting planes $\mathbf{G}$. In this expression $V_{\mathbf{G}}$ is the Fourier component of the potential of silicon corresponding to $\mathbf{G}$, $\Lambda_0=\pi\hbar^2k_0\cos\theta_B/|V_{\mathbf{G}}|$ is the pendellösung length, and d_{hkl} is the spacing between the diffracting lattice planes. Therefore, y is twice as sensitive to small variations in wavelength at the shorter wavelengths. Furthermore, the experimentally determined values of the gravitationally induced phase shift differ from the theoretical values by much

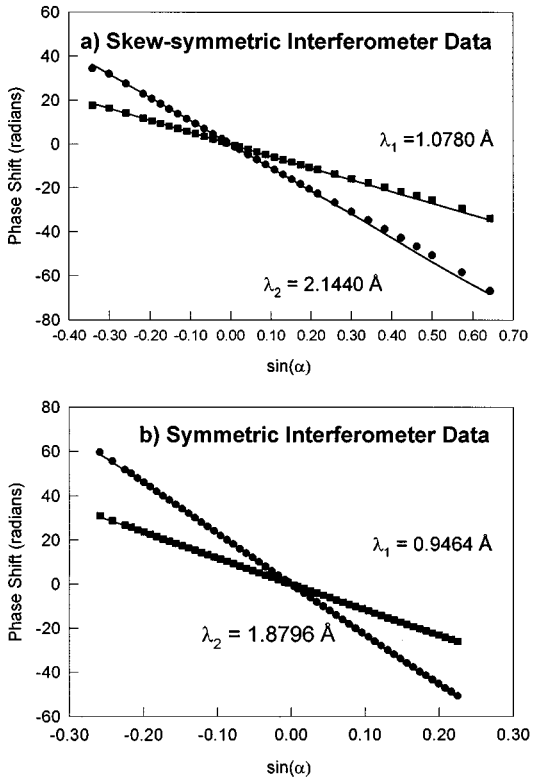

FIG. 19. Graphical representation of the data of Fig. 15 using (a) the skew-symmetric interferometer and (b) the symmetric interferometer pointwise corrected for bending effects. The solid curves are the gravity phase shifts expected from theory.

less than the size of the dynamical diffraction correction, suggesting that the effects of dynamical diffraction are being damped in some manner.

Another, less likely source for the discrepancy is a difference in the way in which centrifugal force acts in classical and quantum mechanics. As yet the effects of centrifugal force on the quantum-mechanical phase have not been studied experimentally except as a correction to COW-type experiments such as this where it is expected to be a contribution that is nearly at the resolution of the measurement. While it is impossible to study the effects of the Earth's gravity independent of centrifugal acceleration, the relative size of these two effects can be determined by studying systems such as the phase shifts due to the sun and the moon where the magnitudes of the inertial forces are in different proportions to the gravitational forces than in the system of the rotating Earth alone.

VI. FUTURE WORK

If the coupling of strains to dynamical diffraction effects is the source of the discrepancies, then it may be possible to reduce them by floating the interferometer in a neutron-transparent solution of the same density as has been done in experiment to measure the inertial and gravitational effective masses of diffracting neutrons [28,29] or by modifying the apparatus so that the interferometer is rotated about an axis of elastic symmetry. Both of these methods would have the effect of reducing the dependence of bending and strain on the tilt angle but would do nothing to counteract the coupling

of the constant, baseline strains, and distortions with the dynamical diffraction correction. The experiment could also be performed with an interferometer with blades thinner in proportion to its length to reduce the size of the dynamical diffraction correction. This would make the interferometer less rigid and thus more susceptible to bending, but this problem could be ameliorated by using the techniques described above. Of course performing the experiment with longer wavelength neutrons would be helpful by increasing the size of the gravitational phase shift relative to other effects while at the same time decreasing the size of the bending correction and the sensitivity of the dynamical diffraction correction to variations in the interferometer.

It may also be necessary to modify the experiment to change the form of the dynamical diffraction correction. This can be done by performing the experiment using more collimated, more monochromatic beams, like those produced using nearly perfect crystals in the monochromator, or by using entrance and exit slits on the interferometer to restrict the wavelength distribution of neutrons along a particular direction that can contribute to the interferogram. It may also be informative to perform the experiment with a two-blade interferometer or a three-blade LLL interferometer in the focusing geometry. Since the gravity-induced phase shift is the result of the neutron spending more time in a higher potential along one path and not actually the area, it would also be interesting to perform the experiment using a neutron interferometer in the Michelson geometry if these become available. Use of this geometry would have the added benefit of completely decoupling the Sagnac effect as there is no enclosed area in the interferometer and thus no Sagnac effect.

VII. CONCLUSIONS AND CONNECTIONS

After careful analysis, tantalizing and significant discrepancies remain between the phase shift due to gravity as measured by experiment and that predicted theoretically. The experimentally obtained values for the gravitationally induced phase factor u were lower than the theoretically expected value by 1.5% for the skew-symmetric interferometer data and 0.8% for the symmetric interferometer data in measurements with relative uncertainties of 0.12% and 0.11%, respectively. Since the discrepancy is different in relative magnitude for the two different interferometers when compared to both the theoretical predictions and the size of the dynamical diffraction corrections, it appears to be related to the interferometer and its mounting. Although these discrepancies appear to be related to the way in which dynamical diffraction interacts with bending and strains in the interferometer, they may also represent a difference between the ways in which gravity acts in classical and quantum mechanics. Before any quantitative conclusions can be reached about the role of the equivalence principle in nonrelativistic quantum mechanics, this discrepancy must either be proven to be due to differences in the gravitational potential between classical and quantum mechanics, or understood as a result of other, unaccounted for experimental parameters and eliminated.

In conclusion, we would like to make a few comments on the Sagnac effect for light, and also on the possibility of observing the gravity-induced phase shift for light. As pointed out by Dresden and Yang [30], the formula [17] for the Sagnac phase shift can be written as

$$\Delta\Phi_{\text{Sagnac}} = 2\frac{k}{v_0}\mathbf{\Omega}\cdot\mathbf{A}_0 . \tag{34}$$

This is correct to first order in Ω, since the neutron's momentum $\hbar k = m_i v_0$, thus $m_i/\hbar = k/v_0$. For photons the velocity $v_0 = c$, the velocity of light. Thus, using the same perfect crystal interferometer for x-ray photons of the same wavelength as our neutrons, the expected phase shift would be a factor of v_0/c smaller than for neutrons. For a wavelength $\lambda = 2$ Å, $v_0/c \approx 0.67\times10^{-5}$, so that $\Delta\Phi_{\text{Sagnac}}(\text{x rays}) = (v_0/c)\Delta\Phi_{\text{Sagnac}}(\text{neutrons}) \approx 1.5\times10^{-5}$ rad for the interferometer ($A_0 = 15.6$ cm^2) used in the original Sagnac effect experiment [2]. Even for an interferometer of linear dimensions 10 times larger (area 100 times larger), which appears feasible, the Sagnac phase shift for x rays would only be 1.5 mrad, presenting an experimental challenge to observe. Of course, if there were a scheme to allow the photons to go around the interferometer many times, as in the ring-laser gyroscope, the conclusion would be quite different. The perfect crystal resonant cavities as described by Rostomyan *et al.* [31] provide an example of such a scheme.

Recently, Mannheim [32] has pointed out that the COW formula (13) for the gravity-induced phase shift can be written in the form

$$\Delta\Phi_{\text{grav}}(\alpha) = -\pi g A_0 \sin\alpha/\lambda v_0^2, \tag{35}$$

if one again makes the replacement $m/\hbar = k/v_0$. Furthermore, he shows using a fully covariant analysis and the nonrelativistic reduction of the Klein-Gordon equation, that the phase shift formula for classical light is identical to Eq. (35) if we replace the neutron velocity v_0 by c. This realization shows us again that the COW effect is really a gravitational redshift for massive particles. For x-ray photons of the same wavelength as our neutrons, we have $\Delta\Phi_{\text{grav}}(\text{x rays}) = (v_0/c)^2\Delta\Phi_{\text{grav}}(\text{neutrons})$. For $\lambda = 2$ Å, $(v_0/c)^2 \approx 0.44\times10^{-10}$, so that observing the COW effect with x rays would be quite difficult indeed, but not totally inconceivable. Suppose we use 0.1-Å x rays and had an interferometer 10 m$\times$10 m, then $\Delta\Phi_{\text{grav}}(\text{x rays}) = 0.6$ mrad. Clearly, such an experiment would take some technological development.

We see in the above numerical examples the considerable sensitivity of the neutron interferometer to rotation and gravity. This has provided the motivation for the current activity in using atom beam interferometers [8,33] for ultrahigh sensitivity accelerometers and gyroscopes, as suggested by Clauser [34] about 10 years ago.

Recently, Ahluwalia and Burgard have investigated the effects of gravitationally induced quantum phase shifts in neutrino oscillations [35]. In the neighborhood of a 1.4 solar-mass neutron star they find that the gravity-induced phases are roughly 20% of their kinematical counterparts.

A preliminary account of the two-wavelength gravity-induced phase-shift experiment discussed in detail in this paper was given at the Neutron Optics Kumatori '96 conference [36].

ACKNOWLEDGMENTS

We are grateful to R. D. Deslattes for his assistance in performing the measurement of the orientation of the crystal planes of the skew-symmetric interferometer and to B. Mashhoon and B. DeFacio for several informative discussions. We would also like to acknowledge the assistance of K. Hoag during the early phases of this experiment. This work was supported by the Physics Division of the National Science Foundation through Grant No. 9024608. K.C.L. received additional support through the United States Department of Education.

[1] R. Colella, A. W. Overhauser, and S. A. Werner, Phys. Rev. Lett. **34**, 1472 (1975).
[2] J.-L. Staudenmann, S. A. Werner, R. Colella, and A. W. Overhauser, Phys. Rev. A **21**, 1419 (1980).
[3] For an early review of the significance of these experiments see D. M. Greenberger and A. W. Overhauser, Rev. Mod. Phys. **51**, 43 (1979). For additional theoretical insights and analysis see L. Stodolsky, Gen. Relativ. Gravit. **11**, 391 (1979); J. Anandan, Nuovo Cimento A **53**, 221 (1979); J. Anandan, Phys. Rev. D **30**, 1615 (1984); E. Fabri and L. E. Picasso, Phys. Lett. A **119**, 268 (1986); E. Fabri and L. E. Picasso, Phys. Rev. A **39**, 4641 (1989); J. Anandan and H. R. Brown, Found. Phys. **25**, 349 (1995); J. Audretsch and C. Lämmerzhal, J. Phys. A **16**, 2457 (1983); Y. Takahashi, Phys. Lett. A **121**, 381 (1987).
[4] P. G. Roll, R. Krotov, and R. H. Dicke, Ann. Phys. (N.Y.) **26**, 442 (1967).
[5] L. Koester, Phys. Rev. D **14**, 907 (1975).
[6] S. A. Werner, H. Kaiser, M. Arif, and R. Clothier, Physica B **151**, 22 (1988).
[7] S. A. Werner, Class. Quantum Grav. **11**, A207 (1994); D. L. Jacobson, doctoral dissertation, University of Missouri Columbia, 1996 (unpublished).
[8] M. Kasevich and C. Chu, Appl. Phys. B **54**, 321 (1992).
[9] M. Arif, M. S. Dewey, G. L. Greene, D. Jacobson, and S. A. Werner, Phys. Lett. A **184**, 154 (1994).
[10] G. P. Woollard and J. C. Rose, *International Gravity Measurements* (George Banta Company, Inc., Menasha, Wisconsin, 1963), p. 99.
[11] G. I. Opat (unpublished).
[12] P. A. M. Dirac, Rev. Mod. Phys. **17**, 195 (1945).
[13] R. P. Feynman, Rev. Mod. Phys. **20**, 367 (1948).
[14] M. G. Sagnac, C. R. Acad. Sci. **157**, 708 (1913); **157**, 1410 (1913); L. A. Page, Phys. Rev. Lett. **35**, 543 (1975).
[15] J. Anandan, Phys. Rev. D **15**, 1448 (1977); Phys. Rev. D **24**, 338 (1981).
[16] L. Stodolsky, in *Neutron Interferometry*, edited by U. Bonse and H. Rauch (Clarendon Press, New York, 1979), p. 313.
[17] H. P. Layer and G. L. Greene, Phys. Lett. A **155**, 450 (1991).
[18] D. Petrascheck, in *Neutron Interferometry* (Ref. [16]), p. 108; D. Petrascheck and R. Folk, Phys. Status Solidi A **36**, 147 (1976).
[19] M. A. Horne, Physica B **137**, 260 (1986).
[20] O. Motrunich, B. E. Allman, K. C. Littrell, and S. A. Werner (unpublished).
[21] U. Bonse and T. Wroblewski, Phys. Rev. Lett. **51**, 1401 (1983).
[22] H. Kaiser, S. A. Werner, and E. A. George, Phys. Rev. Lett. **50**, 563 (1983).
[23] R. Clothier, H. Kaiser, S. A. Werner, H. Rauch, and H. Wölwitsch, Phys. Rev. A **44**, 5357 (1991).
[24] D. L. Jacobson, S. A. Werner, and H. Rauch, Phys. Rev. A **49**, 3196 (1994).
[25] S. A. Werner, H. Kaiser, M. Arif, H.-C. Hu, and R. Berliner, Physica B **136**, 137 (1986).
[26] S. A. Werner, J.-L. Staudenmann, and R. Colella, Phys. Rev. Lett. **42**, 1103 (1979).
[27] D. K. Atwood, M. A. Horne, C. G. Shull, and J. A. Arthur, Phys. Rev. Lett. **52**, 1673 (1984).
[28] K. Raum, M. Koellner, A. Zeilinger, M. Arif, and R. Gähler, Phys. Rev. Lett. **74**, 2859 (1995).
[29] K. Raum, M. Weber, R. Gähler, and A. Zeilinger, J. Phys. Soc. Jpn. **65A**, 277 (1997).
[30] M. Dresden and C. N. Yang, Phys. Rev. D **20**, 1846 (1979).
[31] A. H. Rostomyan, P. H. Bezirganyan, and A. M. Rostomyan, Phys. Status Solidi A **116**, 483 (1989); **116**, 493 (1989); A. H. Rostomyan and A. M. Rostomyan, Phys. Status Solidi A **126**, 29 (1989).
[32] P. D. Mannheim (unpublished).
[33] J. Schmiedmayer, M. S. Chapman, C. R. Ekstrom, T. D. Hammond, D. W. Kieth, A. Lenef, R. A. Rubenstein, E. T. Smith, D. E. Pritchard, *Atom Interferometry*, *Advances in Atomic and Molecular Physics*, edited by Paul R. Berman (Academic, San Diego, 1997), Chap. 1, pp. 2–83.
[34] J. F. Clauser, Physica B **151**, 262 (1988).
[35] D. V. Ahluwalia and C. Burgard, Gen. Relativ. Gravit. **28**, 1161 (1996).
[36] K. Littrell, B. Allman, K. Hoag, and S. Werner, J. Phys. Soc. Jpn. **65A**, 86 (1997).